Journal of Magnetism and Magnetic Materials 424 (2017) 298–303

Contents lists available at ScienceDirect

Journal of Magnetism and Magnetic Materials

journal homepage: www.elsevier.com/locate/jmmm

Crystallographic parameters of magnetic $Pr_2Fe_{14-x}Co_xB$-type alloys determined using anomalous x-ray diffraction with synchrotron radiation

E. Galego*, M.M. Serna, L.V. Ramanathan, R.N. Faria

Energy and Nuclear Research Institute, Materials Science and Technology Center, São Paulo, Brazil

ARTICLE INFO

Keywords:
Rare earth alloys
Magnetic powders
Anomalous x-ray diffraction
Synchrotron radiation, crystallographic parameters

ABSTRACT

Anomalous x-ray synchrotron diffraction was used to determine the crystallographic parameters of PrFeCoB-based magnetic alloys. The effect of cobalt concentration on the crystallographic parameters of the magnetically hard $Pr_2Fe_{14-x}Co_xB$ phase was studied. The results indicate that addition of cobalt has a marked effect on crystal structure. Variation of the *c* parameter decreased twice as much as the *a* parameter with increase in Co content. The positions of inequivalent atoms of the magnetically hard matrix phase ϕ in the Pr-based alloys were determined using Rietveld refinement. This permitted determination of the relative distance of each inequivalent atom from its nearest neighbors. Cobalt occupied the $16k_2$ site and Fe had a tendency to occupy the $8j_2$ sites located between the Kagomé layers.

1. Introduction

It is well known that the Curie temperature of the $Pr_2Fe_{14-x}Co_xB$ system is markedly influenced by the Co content (x). Pedziwiatr et al. showed that at low Co concentrations ($x \leq 6$) in the $Pr_2Fe_{14-x}Co_xB$ alloy, the Curie temperature increased by 50 K for each Fe atom that was substituted, whereas at higher Co concentrations ($x > 6$) the increase of Curie temperature was only 14 K per substituted Fe atom [1]. This variation can be attributed to non-random substitution of Fe by Co in the crystal structure, because the Curie temperature is determined by exchange interactions. $Pr_2Fe_{14}B$ has a tetragonal structure of type $P4_2/mnm$ space group with six inequivalent Fe sites, namely: 4*e*, 4*c*, $8j_1$, $8j_2$, $16k_1$ and $16k_2$. Co can substitute Fe over the entire range in $Pr_2(Fe_{14-x}Co_x)B$ [1–3]. The $16k_2$ site is similar to the *f* site (dumb-bell bond) in the structure of RE_3Fe_{17} (RE: rare earth) and studies related to substitution of Fe by Co indicated that Fe preferred this site. Therefore a similar behavior was expected with $Pr_2Fe_{14}B$, but the experimentally determined intensity of the Fe sites in Mössbauer spectra of $Nd_2(Co_{14-x}Fe_x)B$ was quite different [2–4]. This observation could be attributed to the strong preference of Fe to occupy the $8j_2$ site and to avoid the $16k_2$ site. Both sites have a considerable number of 3d neighbors. However, the distances among nearest neighbors of the $8j_2$ site are relatively larger than those of the $16k_2$ site, indicating that substitution can be controlled by atom size. Besides atom size, bond strength also influences the substitution process in a manner where Co has a strong preference to occupy atomic positions with more RE nearest neighbors, thus leaving Fe in the $8j_2$ position with only two RE atoms as nearest neighbors [5,6].

Besides substituting Fe with Co, other elements are essential to further improve the magnetic behavior of these alloys [7–19]. These compounds contain the magnetically hard phase ϕ (the main phase) in alloys for permanent magnets. To exhibit hard magnetic properties, these alloys are non-stoichiometric and contain small amounts of several transition metals or refractory elements [11,12,15,20–25]. These alloys contain some rare earth element in excess, and boron to achieve high magnetically hard properties. The excess of the added element gets incorporated in phases at grain boundaries, necessary for magnetic isolation of the ϕ grains, which form only in stoichiometric proportion (2-14-1). Very small amounts of Nb, Zr and Ga have been also added to induce anisotropy [9,12–14].

In this study, substitution of Fe with different amounts of Co has been attempted to alter the crystallographic parameters of $Pr_2Fe_{14}B$-based permanent magnet alloys. A very small amount of Nb has been also added to the alloys, to induce some anisotropy. Even though Nb substitutes Pr in the crystal structure, its role has not been considered in this study, because the amount of Nb is below the detection limit of x-ray analysis. These alloys were investigated by scanning x-ray diffraction (XRD) analysis using synchrotron radiation with energies of 7.0892(5) keV and 7.9989(3) keV. Synchrotron radiation has a continuous spectrum from which a single wavelength can be selected using a monochromator. This enables a specific element to be 'highlighted'. This is known as the 'contrast variation technique' where an anomalous dispersion of x-rays is used, and this is a useful tool to study site occupancy for neighboring elements in periodic table [26–28]. The

* Corresponding author.
E-mail address: egalego@ipen.br (E. Galego).

http://dx.doi.org/10.1016/j.jmmm.2016.10.070
Received 7 April 2016; Received in revised form 4 October 2016; Accepted 15 October 2016
Available online 15 October 2016
0304-8853/

Table 1
Composition of the as-cast $Pr_{14}Fe_{bal}Co_xB_6$ alloys.

Substitutional amount X (at%)	Analyzed composition (wt%)				
	Pr	*Fe*	*Co*	*B*	*Nb*
0	30.11	68.58	–	0.97	0.14
4	30.05	65.16	3.58	0.97	0.15
8	30.29	61.27	7.15	0.96	0.15
12	30.14	57.71	10.83	0.98	0.15
16	30.35	54.11	14.34	0.96	0.14

scattering factor f_O of an atom is proportional to the number of electrons it has. However, when a wavelength is selected that is in the vicinity of the absorption edge, the scattering factor changes due to anomalous dispersion. In this case, the real (f') and the imaginary (f'') components of the anomalous dispersion term become significant. Therefore the scattering factor is described as a complex number, $f = f_O + f' + f''$, where f' and f'' can be attributed to scattering caused by absorption and re-emission of photons, and this results in a phase shift [29,30]. Using this approach, the positions of inequivalent atoms in the magnetically hard matrix phase ϕ of the Pr-based alloys were determined by Rietveld refinement.

2. Material and methods

In this investigation five commercially cast alloys produced by vacuum induction melting were used. These alloys can be represented by the general formula $Pr_{14}Fe_{bal}Co_XB_6$ (X is the substitution or atomic composition of the alloy, at%). The chemical composition in weight percent (wt%) of the as-cast alloys is shown in Table 1. As per the supplier's specification, the alloys contained ≤0.7 wt% neodymium, ≤0.2 wt% aluminium and ≤0.04 wt% silicon as the main impurities. Even though Nb was introduced along with the main elements in the alloy, the amount was very small (0.14 wt%) and was therefore considered as an impurity.

The Co content (x) in the hard magnetic $Pr_2Fe_{14-x}Co_xB$ matrix phase ϕ was calculated using the stoichiometric proportion in the $Pr_2Fe_{14}B$ compound (at%: $Pr_{11.8}Fe_{82.5}B_{5.7}$ or wt%: 26.2Pr-72.8Fe-1B). Fig. 1 shows the graph plotted with the calculated data and employed to estimate the Co concentration (x) in the matrix phase from the weight percentage of Co (X) introduced in the alloys. The x-axis shows both, atomic and weight percentage (at% and wt%). Thus, the alloy $Pr_{14}Fe_{bal}Co_{16}B_6$ (X=16 at% or 14.34 wt%) with maximum Co substitution would contain matrix phase grains with nominal composition of $Pr_2Fe_{11.4}Co_{2.6}B$ (x=2.6). Slightly lower values of x can be expected in

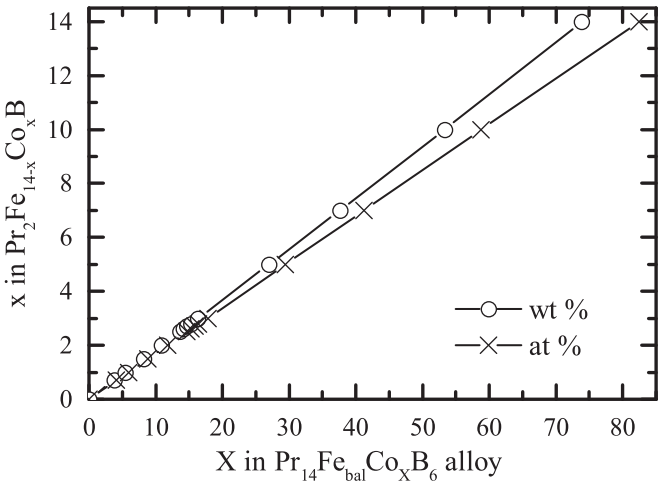

Fig. 1. Relation for estimation of the Co-content (x) in the $Pr_2Fe_{14-x}Co_xB$ magnetic grains of the $Pr_{14}Fe_{bal}Co_XB_6$ alloys.

the alloys due to formation of a small amount of Co containing secondary phases at the grain boundaries. The composition (at% or wt%) in the alloy is identified by the upper case (X) and in the matrix phase by lower case (x). The impurity content and the amount of secondary phases at the grain boundaries in these Pr-based alloys was below the detection limit of 1 wt% in x-ray diffraction analysis, and the x-ray diffraction pattern showed the peaks of the magnetically hard matrix phase only. The scanning electron micrographs of the secondary phases in these alloys have been presented and described in a previous study [31].

The procedure used to prepare the hydrogen processed magnetic powder and the bonded magnet has been described elsewhere [7]. The alloys were vacuum annealed at 1100 °C for 20 h to produce a homogeneous starting material. In this study the powders were milled to 325 mesh for x-ray diffraction analysis. These alloy powders were also isostatically pressed and consolidated by immersion (vacuum impregnated) in low viscosity cyanoacrylate adhesive at 70 °C to form permanent bonded magnets. Magnetic characterization was carried out using a permeameter (accuracy: 2%), after saturation in a pulse field of 6 T. The B_r values were normalized assuming 100% density (7.5 g cm^{-3}) for the sample, and considering a linear relationship between density and B_r [9,14].

X-ray diffraction measurements were used to determine the crystallographic parameters of the $Pr_2Fe_{14-x}Co_xB$ matrix phase of the hydrogen processed alloys. X-ray diffraction data were collected at D10B-XPD beamline of the Brazilian Synchrotron Light Laboratory. X-rays with energies of 7.0892(5) keV and 7.9989(3) keV were selected with a double-bounce Si (111) monochromator. Further on, these energy values will be referred to as 7 keV and 8 keV, respectively. The energy values were chosen taking into consideration the k-edges of Fe (7.112 keV) and Co (7.712 keV), enabling thus the Co form factor to be distinguishable from that of Fe at 7 keV but indistinguishable at 8 keV, as shown in Fig. 2. The values of f' and f'' were calculated by the *Fprime* software [32]. The diffractometer used in this study had a parallel geometry (slits: 3 mm for scattering and 1 mm for receiving) with a 1 m radius goniometer. Measurements of instrument-induced-widening were carried out using a Si standard (NIST-640C). Step-scanning was carried out at the rate of 0.01 degree per step and the time base was normalized to incident beam monitor counts.

The general structure analysis system (GSAS) [33] and its graphical user interface EXPGUI [34] were used to refine the powder diffraction patterns. The model proposed by Herbst and Yelon [35] (space group P42/mmm (136) with a = b =8.796(1) Å and c =12.228(1) Å – ICSD:60517) was used as the initial structural model to determine the crystallographic structure related parameters of the magnetically hard $Pr_2Fe_{14-x}Co_xB$ matrix phase. Using this approach, the lattice parameters, the atom positions, and the percentage of substitution of each Fe site by Co atoms were determined.

3. Results and discussion

Table 2 summarizes the magnetic properties as well as the estimated composition of the matrix phase of the Pr-based bonded magnets prepared using the different alloys in their annealed state. The best remanence (845 ± 10 mT), intrinsic coercivity (946 ± 11 kAm^{-1}) and energy product (140 ± 1 kJm^{-3}) were observed in magnets produced using the $Pr_{14}Fe_{bal}Co_4B_6$ alloy. The squareness factor (0.45) was slightly better in the $Pr_{14}Fe_{bal}Co_8B_6$ bonded permanent magnet. Thus, good magnetic properties could be achieved in alloys containing 4 and 8 at% Co. Addition of higher amounts of Co resulted in an overall decrease in magnetic properties, even though the Curie temperature of the magnetic alloy increased at a constant rate of 11 K per at% Co [16].

Refined x-ray diffraction patterns of the $Pr_{14}Fe_{bal}B_6$ and $Pr_{14}Fe_{bal}Co_{16}B_6$ alloys using monochromatic synchrotron radiation at 7 keV and 8 keV are shown in Figs. 3 and 4. The variations observed in integrated intensities in the x-ray diffraction patterns are due to

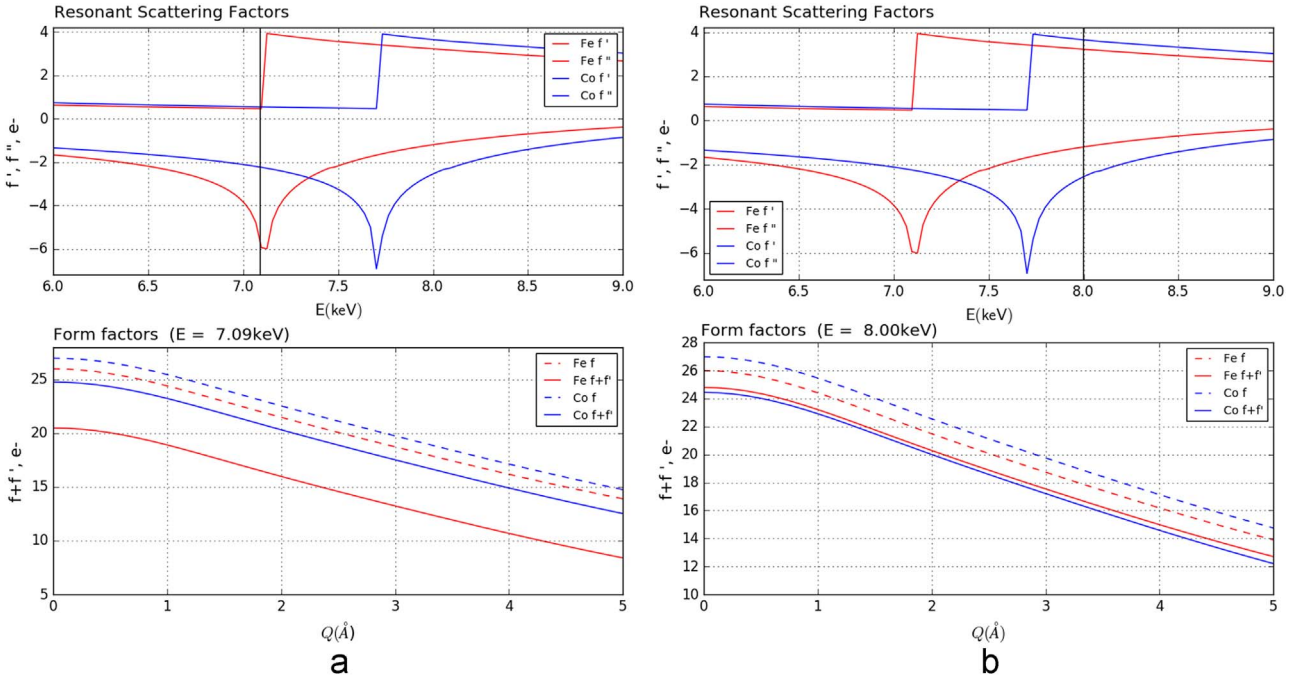

Fig. 2. Resonant scattering and form factors for Fe and Co at (a) 7 keV and (b) 8 keV [32].

substitution of Fe by Co in the structure. In the following expression for integrated intensity, F_{hkl} is the structural amplitude of the *hkl* reflection:

$$F_{hkl} = \sum_{j=1}^{n} g^j t^j(s) f^j(s) e^{2\pi i(hx^j + ky^j + lz^j)}$$

where n is the number of atoms in the unit cell, s is $\sin\Theta_{hkl}/\lambda$, g^j is extent of occupation of the j^{th} atom (g^j =1 for a fully occupied site), t^j is the temperature factor, and $f^j(s)$ is the atomic scattering factor. In this study we used the resonant scattering factor (or anomalous dispersion) to refine g^j for Co and Fe. The goodness-of-fit indicators for all refinements were $\chi^2 < 1.68$, $R_{wp} < 3.17\%$ and $R_F^2 < 4.01\%$. This could also be evaluated by visual inspection of the fitting. The R_F^2 values, after refinement for energies between 7 keV and 8 keV for each alloy composition was less than 1%, indicating good agreement with the structural model.

Table 3 summarizes the lattice parameters of the magnetically hard matrix phase ϕ of the Pr-based alloys. The decrease in lattice parameters with increase in Co content indicates that introduction of this element in the magnetically hard phase was proportional to its concentration in the alloy. The *c* parameter decreased twice as much as the *a* parameter with increase in Co concentration, and this is clearly observed in Fig. 5. This behavior is consistent with the results of other studies of $Pr_2Fe_{14-x}Co_xB$ compounds which reported that Co had a tendency to yield planar anisotropy [1–6]. The decrease in lattice parameter causes a change in the position of the atom sites, and consequently, in the inter-atomic distances, essential for exchange interactions related to the Curie temperature.

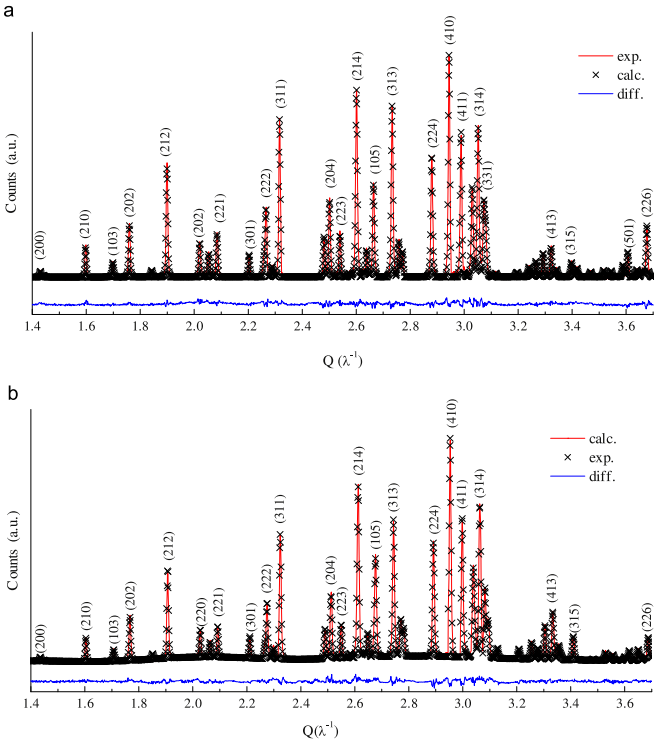

Fig. 3. X-ray diffraction patterns of $Pr_{14}Fe_{bal}B_6$ (a) 7 keV, (b) 8 keV.

Table 2
Magnetic properties and estimated composition of the ϕ phase of the magnets prepared with the alloy annealed under high vacuum. Permeameter measurements were carried out at room temperature after saturation in a 6 T magnetic pulse field..

Composition of the alloys (at%)	B_r (mT)	$_iH_c$ (kAm^{-1})	$_bH_c$ (kAm^{-1})	$(BH)_{max}$ (kJ/m^3)	SF (ratio)	ϕ phase ($Pr_2Fe_{14}Co_xB$)
$Pr_{14}Fe_{bal}B_6$	801 ± 10	859 ± 12	429 ± 9	96 ± 9	0.39	$Pr_2Fe_{14}B$
$Pr_{14}Fe_{bal}Co_4B_6$	845 ± 10	946 ± 11	510 ± 3	140 ± 1	0.41	$Pr_2Fe_{13.3}Co_{0.7}B$
$Pr_{14}Fe_{bal}Co_8B_6$	803 ± 14	872 ± 14	493 ± 9	135 ± 5	0.45	$Pr_2Fe_{12.5}Co_{1.4}B$
$Pr_{14}Fe_{bal}Co_{12}B_6$	753 ± 11	779 ± 10	493 ± 4	121 ± 2	0.42	$Pr_2Fe_{12.0}Co_{2.0}B$
$Pr_{14}Fe_{bal}Co_{16}B_6$	701 ± 12	700 ± 11	446 ± 6	47 ± 2	0.25	$Pr_2Fe_{11.3}Co_{2.7}B$

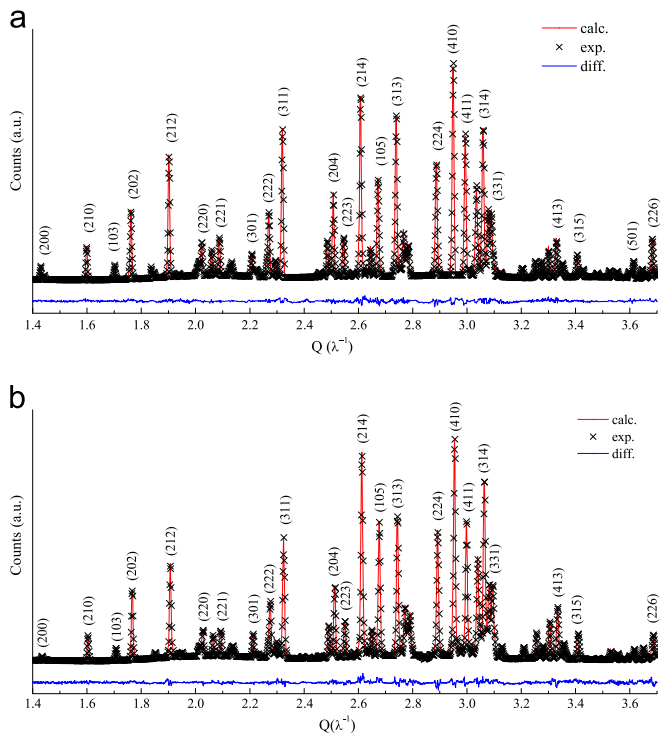

Fig. 4. X-ray diffraction patterns of $Pr_{14}Fe_{bal}Co_{16}B_6$ (a) 7 keV and (b) 8 keV.

Table 3
Lattice parameters of the $Pr_{14}Fe_{bal}Co_XB_6$alloys.

Composition of the alloy	a (Å)	c (Å)
$Pr_{14}Fe_{bal}B_6$	8.80410(6)	12.24679(15)
$Pr_{14}Fe_{bal}Co_4B_6$	8.80152(6)	12.23759(14)
$Pr_{14}Fe_{bal}Co_8B_6$	8.79607(5)	12.22539(12)
$Pr_{14}Fe_{bal}Co_{12}B_6$	8.78866(5)	12.21119(11)
$Pr_{14}Fe_{bal}Co_{16}B_6$	8.78309(6)	12.19957(14)

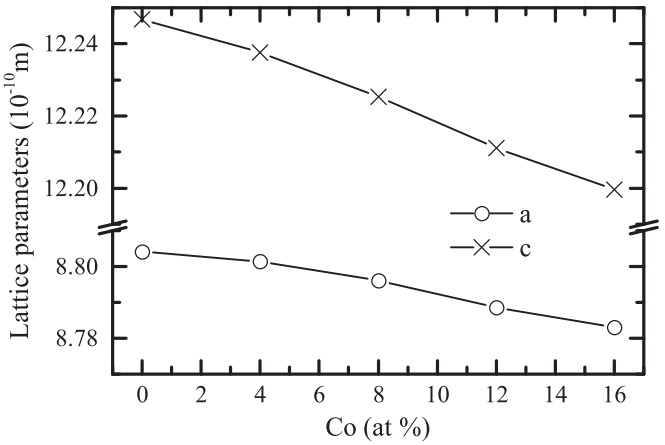

Fig. 5. Variation of lattice parameters in the $Pr_{14}Fe_{bal}Co_XB_6$ alloys.

The values of fractional occupancy (FO) of all inequivalent sites for Co atoms in the crystal structure of the magnetically hard phase are shown in Table 4 after Rietveld refinement. This table also includes the fraction of atoms (FA), which is the product of FO and the number of atoms in the site. For instance: FA of the Co atoms at $16k_1$ site is equal to 0.7 (16×0.0440). Cobalt occupies preferentially the $16k_2$ site and this is in agreement with previous investigations [1,3,4]. Bolzoni *et al.* reported that Fe has a tendency to occupy the $8j_2$ sites located between the Kagomé layers formed for Fe [6,19]. Van Noort and Buschow [6]

Table 4
Values of fraction occupancy (FO) and fraction of atoms (FA) of Co..

$Pr_{14}Fe_{bal-x}Co_XB_6Nb_{0,1}$.	X=4		X=8		X=12		X=16	
Site	***FO***	***FA***	***FO***	***FA***	***FO***	***FA***	***FO***	***FA***
$16k_1$	0.0440	0.70	0.1110	1.76	0.0550	0.88	0.2029	3.25
$16k_2$	0.0950	1.52	0.1728	2.76	0.2602	4.16	0.2924	4.68
$8j_1$	0.1122	0.90	0.2141	1.71	0.3735	2.99	0.4650	3.72
$8j_2$	0.0739	0.59	0.1043	0.83	0.2175	1.74	0.0974	0.78
4*e*	0.0094	0.04	0.1452	0.58	0.3395	1.36	0.3443	1.38
4*c*	0.0010	0.00	0.0551	0.22	0.1210	0.48	0.4024	1.61

Table 5
Stoichiometry of $Pr_2Fe_{14-x}Co_xB$ phase.

$Pr_{14}Fe_{56-x}Co_XB_4$	Fe	Co
X = 4	53.232(2)	3.754(2)
X = 8	46.350(2)	7.889(2)
X = 12	44.387(2)	11.613(2)
X = 16	40.590(2)	15.411(2)

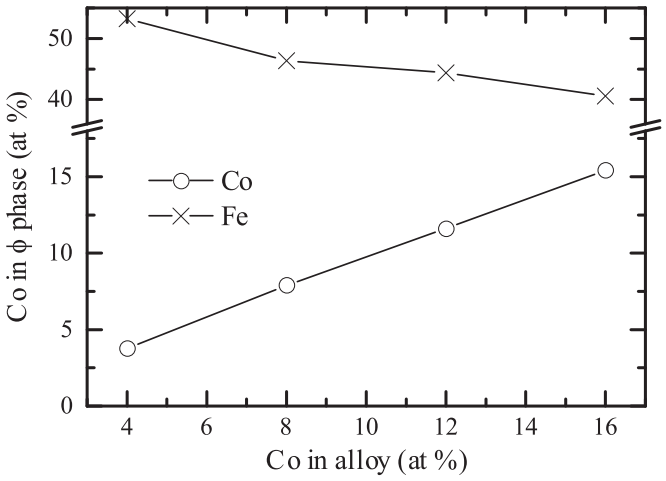

Fig. 6. Stoichiometry variation of the Fe and Co in $Pr_2Fe_{14-x}Co_xB$ phase.

Table 6
Position of $8j_2$ and $16k_1$ sites in $Pr_{14}Fe_{bal}B_6$ phase in $Pr_{14}Fe_{bal}Co_{16}B_6$ alloys.

Composition of the alloy	Site	Position		
		x	***y***	***z***
$Pr_{14}Fe_{bal}B_6$	$8j_2$	0.3171(4)	0.3171(4)	0.2462(4)
$Pr_{14}Fe_{bal}Co_{16}B_6$	$8j_2$	0.3178(4)	0.3178(4)	0.2465(4)
$Pr_{14}Fe_{bal}B_6$	$16k_2$	0.0379(4)	0.3609(4)	0.1770(3)
$Pr_{14}Fe_{bal}Co_{16}B_6$	$16k_2$	0,0376(3)	0.3610(3)	0.1763(3)

Table 7
Inter-atomic distances between the Pr sites and $8j_2$ as well as $16k_1$ sites.

Composition of the alloy	Pr site	Site	Atoms	Distance (Å)
$Pr_{14}Fe_{bal}B_6$	*f*	$8j_2$	2	3.071(5)
		$16k_2$	4	3.084(3)
$Pr_{14}Fe_{bal}Co_{16}B_6$	*f*	$8j_2$	2	3.066(5)
		$16k_2$	4	3.069(3)
$Pr_{14}Fe_{bal}B_6$	*g*	$8j_2$	2	3.151(5)
		$16k_2$	4	3.054(3)
$Pr_{14}Fe_{bal}Co_{16}B_6$	*g*	$8j_2$	2	3.133(5)
		$16k_2$	4	3.288(3)

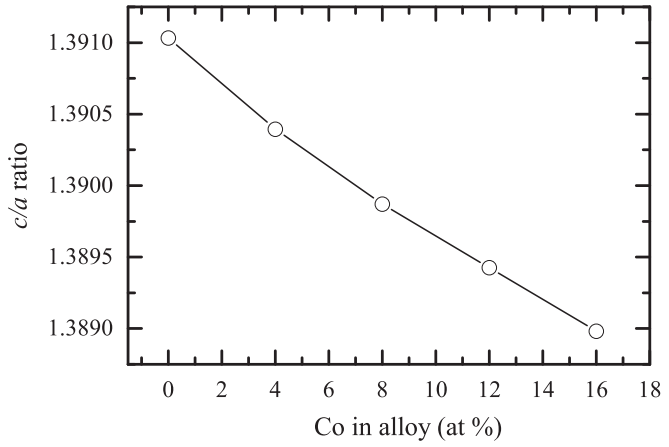

Fig. 7. Non-linear behavior of the c/a ratio with Co in the alloy.

suggested that on the basis of the atom size and electronegativity, the Fe atoms prefer larger sites with fewer Pr atoms as first neighbors. As a consequence, the Co atoms occupy the inverse sites of those preferred by Fe, with a higher number of Pr atoms as first neighbors. Furthermore, compared to results reported in the literature, this study also shows that initially Fe is substituted by Co at other sites in a non-systematic manner, indicating that electronegativity is a determining factor in substitutions.

Table 5 shows stoichiometry of the magnetically hard phase and this was determined using FO of the Co atom. It can be seen that in the different alloys, all the Co atoms were not incorporated in the magnetic phase, indicating that some Co formed secondary phases at the grain boundaries. Proof of this was observed and has been presented elsewhere [31]. The trend can be easily seen in Fig. 6.

Table 6 summarizes the position of inequivalent atoms of the magnetically hard matrix phase ϕ in the Pr-based alloys. This was determined by Rietveld refinement. This enabled determination of the relative distance of each inequivalent atom from its nearest neighbors. There was no significant change in the position of $8j_2$, indicating that substitution with Co at this site resulted in no significant change in the crystallographic parameters related to this position. Conversely at the $16k_2$ site, alteration of the z position was observed as shown in Table 6, which is in agreement with the decrease in lattice parameter discussed earlier. Table 7 summarizes the inter-atomic distances between the base atom and neighbors for the magnetic matrix phase ϕ of the Pr-based alloys. Co has a tendency to preferentially occupy (with some still randomly distributed) crystallographic sites with many nearest neighbor elements that have a 3d layer, such as Fe [1]. The changes in the inter-atomic distances in the $Pr_2Fe_{14-x}Co_xB$ system resulted in alterations in magnetic exchange interactions involving different 3d sites. The decrease in c/a ratio, shown in Fig. 7, corroborates the preference of Co for sites with the strongest 3D-3d exchange interactions that determine, above all, the Curie temperature [36]. The results indicate that accommodation of Co at the $16k_2$ site led to local deformation of the structure with increase in distance between the $16k_2$ site and the Pr g site.

4. Conclusions

X-ray synchrotron diffractometry was used to determine the crystallographic parameters of PrFeCoB-based alloys and a decrease in lattice parameter was observed with increase in Co concentration in the alloy. The c parameter decreased more than the a parameter, and this resulted in a non-linear c/a relationship. The stoichiometric balance between the two atoms (Fe and Co) for each inequivalent site was established. The calculated stoichiometry of all the alloys showed that some of the added Co did not enter the magnetically hard phase ϕ, but remained at the grain boundaries. Preferential substitution of Fe at the $16k_2$ site by Co was observed, which is in agreement with existing literature. Rietveld refinement showed that substitution of Fe by Co at the other sites of the structure was controlled by electronegativity.

Acknowledgements

The authors wish to thank FAPESP and IPEN-CNEN/SP for the financial support and infrastructure made available to carry out this investigation. We also thank the XPD Beamline staff for their help during the experiments carried out at the National Synchrotron Light Laboratory (LNLS), Brazil.

References

[1] A.T. Pedziwiatr, S.Y. Jiang, W.E. Wallace, Structure and magnetism of the $Pr_2Fe_{14-x}Co_xB$ system, J. Magn. Magn. Mater. 62 (1986) 29–35. http://dx.doi.org/10.1016/0304-8853(86)90730-4.

[2] A.T. Pedziwiatr, K. Krawiec, B.F. Bogacz, S. Wróbel, D. Kaczorowski, J. Przewoznik, Mössbauer and calorimetric studies of spin reorientation processes in $Er_{2-x}Pr_xFe_{14}C$, J. Phys. Conf. Ser. (2011) 303 (http://dx.doi:10.1088/1742-6596/303/1/01027).

[3] A.T. Pedziwiatr, W.E. Wallace, Spin phase diagrams for $R_2Fe_{14-x}Co_xB$ systems (R = Y, Gd, Pr, Nd, Tb, Er, Tm), Solis State Commun. 64 (1987) 1017–1019. http://dx.doi.org/10.1016/0038-1098(87)91021-0.

[4] H.M. Van Noort, K.H.J. Buschow, On the site preference of 3d atoms in compounds of the $R_2(Co_{1-x}Fe_x)_{14}B$ type, J. Less Common Met. 113 (1985) L9–L12. http://dx.doi.org/10.1016/0022-5088(85)90160-2.

[5] G.S. Burkhanov, N.B. Kol'chugina, A.A. Lukin, S.K. Godovikov, Y.S. Koshkidko, K. Skotnicova, Studying features of structural state of high-coercivity (Nd, Pr, Dy, Tb)-Fe-B magnetic materials via mössbauer spectroscopy, B. Russ. Acad. Sci. Phys. 79 (2015) 1022–1025. http://dx.doi.org/10.3103/S1062873815080031.

[6] F. Bolzoni, J.M.D. Coey, J. Gavian, D. Givord, O. Moze, L. Pareti, T. Viadieu, Magnetic properties of $Pr_2(Fe_{1-x}Co_x)_{14}B$ compounds, J. Magn. Magn. Mater. 65 (1987) 123–127. http://dx.doi.org/10.1016/0304-8853(87)90316-7.

[7] R.N. Faria, B.E. Davies, D.N. Brown, I.R. Harris, Microstructural and magnetic studies of cast and annealed Nd and PrFeCoBZr alloys and HDDR materials, J. Alloy. Compd. 296 (2000) 223–228. http://dx.doi.org/10.1016/S0925-8388(99)00536-8.

[8] R.N. Faria, J.S. Abbel, I.R. Harris, High coercivity sintered Pr-Fe-B-Cu magnets using the hydrogen decrepitation process, J. Alloy. Compd. 177 (1991) 311–320. http://dx.doi.org/10.1016/0925-8388(91)90084-9.

[9] L.P. Barbosa, H. Takiishi, R.N. Faria, The effect of cobalt content on the microstructure of Pr-Fe-Co-B-Nb alloys and magnetic properties of HDDR magnets, J. Magn. Magn. Mater. 268 (2004) 132–139. http://dx.doi.org/10.1016/S0304-8853(03)00487-6.

[10] N. Cannesan, J.M. LeBreton, A.J. Williams, I.R. Harris, The evolution of the disproportionated microstructure of PrFeB-Based alloys, J. Magn. Magn. Mater. 242 (2002) 1372–1374. http://dx.doi.org/10.1016/S0304-8853(01)01236-7.

[11] O. Gutfleisch, A. Teresiak, B. Gebel, K.H. Muller, N.B. Cannesan, D. Brown, I.R. Harris, Metastable borides and the inducement of texture in $Pr_2Fe_{14}B$-type magnets produced by HDDR, IEEE Trans. Magn. 37 (2001) 2471–2473. http://dx.doi.org/10.1109/20.951206.

[12] N. Cannesan, J.M. LeBreton, A.J. Williams, I.R. Harris, The evolution of the disproportionated microstructure of PrFeB-Based alloys, J. Magn. Magn. Mater. 242 (2002) 1372–1374. http://dx.doi.org/10.1016/S0304-8853(01)01236-7.

[13] R.N. Faria, H. Takiishi, A.R.M. Castro, L.F.C.P. Lima, I. Costa, Chemical micro-analysis of rare-earth-transition metal-boron alloys and magnets using scanning electron microscopy, J. Magn. Magn. Mater. 246 (2002) 351–359. http://dx.doi.org/10.1016/S0304-8853(02)00105-1.

[14] L.P. Barbosa, H. Takiishi, L.F.C.P. Lima, R.N. Faria, The effect of niobium content on the magnetic properties and microstructures of PrFeCoBNb HDDR magnets and alloys, J. Magn. Magn. Mater. 283 (2004) 263–269. http://dx.doi.org/10.1016/j.jmmm.2004.05.032.

[15] E. Galego, H. Takiishi, R.N. Faria, Magnetic properties of Pr-Fe-Co-B bonded HDDR magnets with alloying additions, Mater. Res 10 (2007) 273–277. http://dx.doi.org/10.1590/S1516-14392007000300010.

[16] L.P. Barbosa, H. Takiishi, R.N. Faria, D. Rodrigues, S. Janasi, Curie temperature determination of $Pr_{14}Fe_{79.9-x}Co_xB_6Nb_{0.1}$ permanent magnet alloys, Mater. Sci. Forum 530- 531 (2006) 176–180.

[17] A.F. Petrakov, V.P. Piskorskii, G.S. Burkhanov, M.V. Repina, S.I. Ivanov, Special features of Nd(Pr)-Dy-Fe-Co-B magnets with high content of Co, Met. Sci. Heat. Treat. 54 (2012) 323–329. http://dx.doi.org/10.1007/s11041-012-9506-3.

[18] M. Rajasekhar, D. Akhtar, S. Ram, The effect of substitution of Nd by Pr on the magnetic properties of melt-spun Nd-Fe-B nanocomposite alloys, J. Phys. Appl. Phys. 43 (2010) 135005. http://dx.doi.org/10.1088/0022-3727/43/13/135004.

[19] E.N. Kablov, O.G. Ospennikova, O.A. Bayukov, N.O. Pletnev, I.I. Rezchikova, R.A. Valeev, D.V. Korolev, E.I. Kunitsyna, V.P. Piskorskii, R.B. Morgunov, Effect of stoichiometry of Fe and Co on the temperature stability of the magnetic anisotropy in Pr-Dy-Fe-Co-B alloys, Phys. Solid State 57 (2015) 1362–1365. http://dx.doi.org/10.1134/S1063783415070161.

[20] A. Kowalczyk, Magnetic and crystallographic properties of substituted $Pr_2Fe_{14-x}M_xB$ compounds (M = Si, Ga, Cr and Cu), J. Magn. Magn. Mater. 82 (1989) L1–L4. http://dx.doi.org/10.1016/0304-8853(89)90054-1.
[21] R. Nakayama, T. Takeshita, M. Itakura, N. Kuwano, K. Oki, Magnetic-properties and microstructures of the Nd-Fe-B magnet powder produced by hydrogen treatment, J. Appl. Phys. 70 (1991) 3770–3774. http://dx.doi.org/10.1063/1.349232.
[22] R. Nakayama, T. Takeshita, M. Itakura, N. Kuwano, K. Oki, Microstructures and crystallographic orientation of crystalline grains in anisotropic Nd-Fe-Co-B-(Ga or Zr) magnet powders produced by the hydrogenation-decomposition-desorption-recombination process, J. Appl. Phys. 76 (1994) 412–417. http://dx.doi.org/10.1063/1.349232.
[23] T. Takeshita, K. Marimoto, Anisotropic Nd-Fe-B bonded magnets made From HDDR powders, J. Appl. Phys. 79 (1996) 5040–5044. http://dx.doi.org/10.1063/1.361567.
[24] W.Pan, L.Y.Cui, P.Wang, S.X.Zhou, Magnetic Properties of HDDR Processed $(Pr_{1-x}Nd_x)_{13}Fe_{81}B_6$. in: Proceedings of the Fourteenth International Workshop on Rare-Earth Magnets and Their Applications, São Paulo 467, 1996.
[25] Y.B. Kim, W.Y. Jeung, Hydrogen absorption and desorption behavior in Pr-Fe-B type alloys, J. Appl. Phys. 83 (1998) 6405–6407. http://dx.doi.org/10.1063/1.367920.
[26] Y. Waseda, Anomalous X-ray scattering for materials characterization – atomic-scale structure determination, Springer-Verlag, Berlin Heidlberg, 2002.
[27] G. Materlik, C.J. Sparks, K. Fisher, Resonant Anomalous X-ray Scattering: theory and Applications, Elsevier Science, Amsterdam, 1994.
[28] C.E. Williams, R.P. May, A. Guinier, Small-Angle Scattering of X-ray and Neutrons, in: Eric Lifshin (Ed.)X-ray Characterization of Materials, Wiley-VCH Verlag GmbH, Germany, 1999, pp. 211–253.
[29] D.T. Cromer, D.A. Liberman, Relativistic calculation of anomalous scattering factor for X-rays, J. Chem. Phys. 53 (1970) 1891–1898.
[30] D.A. Liberman, Anomalous dispersion calculations near to and on the long-wavelength side of an absorption edge, Acta Cryst. A37 (1981) 267–268. http://dx.doi.org/10.1107/S0567739481000600.
[31] E. Galego, M.M. Serna, R.N. Faria, Evaluation of mean crystallite size on magnetic powder by scanning electron microscopy and synchrotron diffractometry, Mater. Sci. Applic. (2014) 504–511. http://dx.doi.org/10.4236/msa.2014.58055.
[32] R.B.Von Dreele, M.Suchomel, B.H.Toby, Fprime: X-ray Cross-section Estimators, ⟨http://www1.aps.anl.gov/science/scientific-software/fprime⟩ (accessed 25.05.16), 2009.
[33] A.C.Larson, R.B.Von Dreele, General Structure Analysis System (GSAS), Los Alamos National Laboratory Report LAUR 86-748, 2004.
[34] B.H. Toby, EXPGUI, a graphical user interface for GSAS, J. Appl. Cryst. 34 (2001) 210. http://dx.doi.org/10.1107/S0021889801002242.
[35] J.F. Herbst, W.B. Yelon, Crystal and magnetic structure of $Pr_2Fe_{14}B$ and $Dy_2Fe_{14}B$, J. Appl. Phys. 57 (1985) 2343–2345. http://dx.doi.org/10.1063/1.33434.
[36] M.Q. Hung, E.B. Boltich, W.E. Wallace, E. Olwald, Magnetic characteristics of $R_2(Fe, Co)_{14}B$ systems (R = Y, Nd and Ga), J. Magn. Magn. Mater. 60 (1986) 270–274. http://dx.doi.org/10.1016/0304-8853(86)90110-1.